Effects of Grain Scale Heterogeneity on Rock Strength and the Chipping Process

Article *in* International Journal of Geomechanics · December 2012

DOI: 10.1061/(ASCE)GM.1943-5622.0000194

3 authors:

Marlene Villeneuve
University of Canterbury
63 PUBLICATIONS **388** CITATIONS
SEE PROFILE

Mark S. Diederichs
Queen's University
214 PUBLICATIONS **4,354** CITATIONS
SEE PROFILE

P. K. Kaiser
Laurentian University
202 PUBLICATIONS **6,193** CITATIONS
SEE PROFILE

Effects of Grain Scale Heterogeneity on Rock Strength and the Chipping Process

Marlène C. Villeneuve[1]; Mark S. Diederichs[2]; and Peter K. Kaiser[3]

Abstract: Heterogeneity is an important factor controlling fracture initiation, accumulation, and propagation within polycrystalline rock. Internal spatial variability in terms of mineralogy, grain size, and anisotropy affect the yielding process. To investigate these factors, a texture-generating algorithm integrated within a numerical model was developed to create realistic rock analogs and provide user control over geological characteristics including mineral type, grain size, and anisotropic crystal shape. A mineral-specific constitutive model was created and calibrated using published values and real laboratory strength values. Brazilian tensile strength and unconfined compressive strength (UCS) model tests were developed using the finite-difference modeling software *FLAC* to perform parametric analysis of a series of geological characteristics. The results show that the methodology is capable of realistically reproducing damage propagation and failure behavior similar to that observed during laboratory testing. The strength results show trends similar to those found during laboratory testing. This methodology was applied to the simulation of tunnel-boring machine (TBM) cutter excavation to investigate the effect of geomechanical characteristics on the chipping process. **DOI: 10.1061/(ASCE)GM.1943-5622.0000194.**

CE Database subject headings: Numerical models; Compressive strength; Tensile strength; Cracking; Rocks; Excavation; Grains (material).

Author keywords: Numerical modeling; Compressive strength; Brazilian tensile strength; Fracture behavior; Geological characteristics; Heterogeneity; Tunnel-boring machine excavation; Chipping.

Introduction

Traditional analysis techniques in rock engineering aimed at predicting in situ rock behavior during tunnel-boring machine (TBM) tunneling are, for the most part, based on empirical relationships for actual rock behavior considering features of both the excavation and the surrounding geology (Bruland 1998), or on semiempirical relationships between rock mechanics parameters measured by laboratory testing correlated to behavior in physical models and real case histories (Barton 2000; Rostami and Ozdemir 1993). This is true for the specific case of predicting rock fracture both at the excavation scale in terms of wall damage and at the laboratory sample scale. The former is exemplified by the relationship between an empirical ratio (40–50%) of intact unconfined compressive strength (UCS) and tunnel spalling behavior (Kaiser et al. 1995; Martin et al. 1999). The latter is also the scale of TBM cutting tools, for example.

These methods have proved to be adequate in many situations, but there remains a need and desire to understand the rock failure process to be better able to predict rock behavior (Kaiser 2005). One logical avenue would be to employ further laboratory rock strength testing for innumerable situations and observe and compare a rock's underground behavior with the strength test results. Another approach, which was rigorously applied in the 1960s and 1970s (Brace 1960; Brace 1961; Illston et al. 1979; Lama and Vutukuri 1978; Tapponnier and Brace 1976), is to return to fundamental materials science principles to understand the failure process of polycrystalline materials with a variety of physical, elastic, and mechanical properties.

By understanding the fundamentals of how rocks fail, it will be possible to understand the failure process during laboratory testing as well as during excavation and to better relate laboratory test results with in situ behavior. The research presented contains a study on the impact of a set of geological characteristics on in situ rock behavior and its comparison with laboratory strength test values. The aim is to provide a method by which laboratory strength values can be translated into better in situ rock behavior predictions.

The focus here is the failure behavior of intact rock, in particular the creation of new fractures through intact rock as a result of in situ stress induced by the geometry of the excavation or excavating tools. The rocks investigated are massive, crystalline rocks with common mineralogy. The use of the label massive refers to rocks with little to moderate jointing, for example with geological strength index (GSI) > 70 and rock mass rating (RMR) > 75, and a range of in situ stress from low to high. Other researchers have spent considerable effort understanding the behavior of fractured rock masses where the characteristics of discontinuities dominate the behavior (Barton et al. 1974; Bieniawski 1989; Hoek 1994); these rock mass types are not addressed in the present research. This work addresses the characterization of rocks at the mineral grain scale and the impact on macrobehavior.

Numerical modeling of laboratory strength tests has been undertaken using finite-element (Tang and Kaiser 1998; Zhu and Tang 2004; Li et al. 2003) and finite-difference (Chen et al. 2007) codes to examine the failure behavior of heterogeneous rock, with a particular focus on brittle failure. The heterogeneity was either simulated through strength distributions (Tang and Kaiser 1998; Zhu and Tang

[1]Lecturer, Dept. of Geological Sciences, Univ. of Canterbury, Christchurch 8140, New Zealand (corresponding author). E-mail: marlene.villeneuve@canterbury.ac.nz

[2]Professor, Dept. of Geological Sciences and Geological Engineering, Queen's Univ., Kingston, ON, Canada K7L 3N6.

[3]Professor, President, and CEO, Centre for Excellence in Mining Innovation, Laurentian Univ., Sudbury, ON, Canada P2E 2C6.

Note. This manuscript was submitted on March 29, 2011; approved on November 22, 2011; published online on November 24, 2011. Discussion period open until May 1, 2013; separate discussions must be submitted for individual papers. This paper is part of the ***International Journal of Geomechanics***, Vol. 12, No. 6, December 1, 2012. ©ASCE, ISSN 1532-3641/2012/6-632–647/$25.00.

Int. J. Geomech. 2012.12:632-647.

2004) or with digital image simulation (Chen et al. 2007). Neither of these approaches can effectively be used to explicitly perform parametric analysis of geological characteristics, such as mineralogy, grain size, and anisotropy. New developments with hybrid fracture codes (continuum/discontinuum) have the potential to improve the simulation capability (Castelli et al. 2003; Mahabadi et al. 2010; Coggan et al. 2003), especially with respect to fracture initiation, propagation, and coalescence (Shen et al. 2011). The incorporation of realistic quantifiable heterogeneity would benefit these analyses as well.

Numerical modeling of TBM rock cutting has been undertaken using finite-element codes with various geometries, but in general consist of homogeneous or statistically heterogeneous rock block and one or two cutter loaded with a velocity (displacement per step). The goals ranged from geometrical studies (Liu et al. 2002a), rock properties [heterogeneity (Liu et al. 2002a) and grain size (Sulem and Cerrolaza 2002)], and fracture behavior during cutting (Liu et al. 2002b), although one explicitly modeled rock textures.

This paper will demonstrate how numerical modeling of simple continuum strength test models (two-dimensional Brazilian and UCS test models) and the TBM cutting process using *FLAC* (*FLAC*) were used to provide a testing tool for investigating the influence of each parameter on rock fracture, in which varying parameters at the grain scale were explicitly controlled by the user. The results can be used in a comparative fashion to enhance standard characterization methods to include consideration of grain scale mineralogy and fabric.

Numerical Analog for Rock in *FLAC*

To perform a parametric analysis of the impact of geological factors on strength tests, a methodology was developed to explicitly simulate rock textures and geological characteristics at the grain scale. This methodology consists of two parts: a method by which mica, quartz, and feldspar were simulated in a realistic rock aggregate analog based on thin sections of rocks, and the creation of separate constitutive models for each mineral type used in the model.

Rock analogs were simulated by the generation of mineral aggregates using simple geometrical algorithms for generating ellipses. This methodology allows explicit control on aggregate size and orientation through specification of ellipse size and elongated axis orientation. In addition, grain boundaries can also be explicitly generated.

The basic equation for finding the distance, r, from one focus of an ellipse to a point on the edge of the ellipse at angle θ from the long axis, * (Fig. 1), is

$$r = \frac{a(1-e^2)}{1 + e\cos\theta} \tag{1}$$

For the purposes of this research, the angle of the long axis with respect to the horizontal, γ, must have the ability to be varied (Fig. 1). To accommodate this, the basic formula for determining r was modified by determining the necessary angles. First, the γ angle was prescribed or randomly generated within *FLAC* by the FISH code (programming language internal to *FLAC*). Second, the α angle relating the line between the focus and the test element to the horizontal was calculated as

$$\alpha = \tan^{-1}\left[\left(y_{\text{test element}} - y_{\text{focus}}\right)/\left(x_{\text{test element}} - x_{\text{focus}}\right)\right] \tag{2}$$

Third, the θ angle between the long axis and the line between the focus and the test element was calculated as

$$\theta = 180 - \alpha - \gamma \tag{3}$$

Once θ has been determined, it can be used to solve Eq. (1) to obtain the distance, r, between the focus and the ellipse boundary along the line between the focus and the test element. The distance between the test element and the focus, t, was then tested against the distance r to determine whether the test element was inside or outside the ellipse. All test elements that fall within the ellipse were assigned the mineral type being generated. Grain boundaries were assigned to elements on the ellipse boundary, one element in thickness.

Natural crystal and grain geometries were used as the model for generating mineral shapes. Fig. 2 shows that most minerals can either be represented as circles or ellipses. By changing the eccentricity and radius of ellipses, various mineral shapes, orientations,

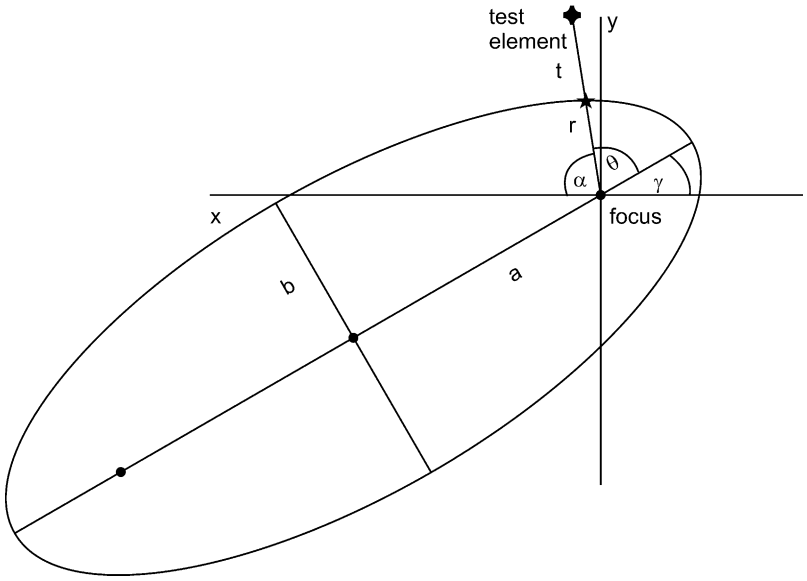

Fig. 1. Schematic of ellipse rotated γ degrees from the horizontal, showing necessary angles for determining r for a test element

Int. J. Geomech. 2012.12:632-647.

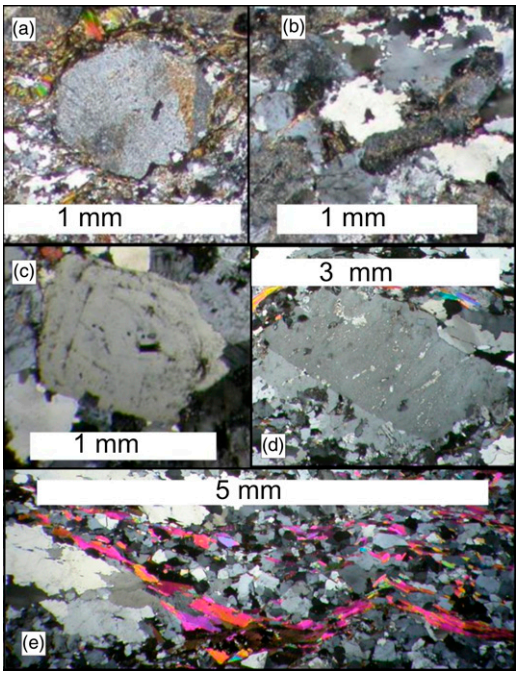

Fig. 2. Photomicrographs of round and elliptical grain shapes: (a) round feldspar; (b) roughly round quartz; (c) slightly elongated feldspar; (d) elongated feldspar; (e) very elongated micas

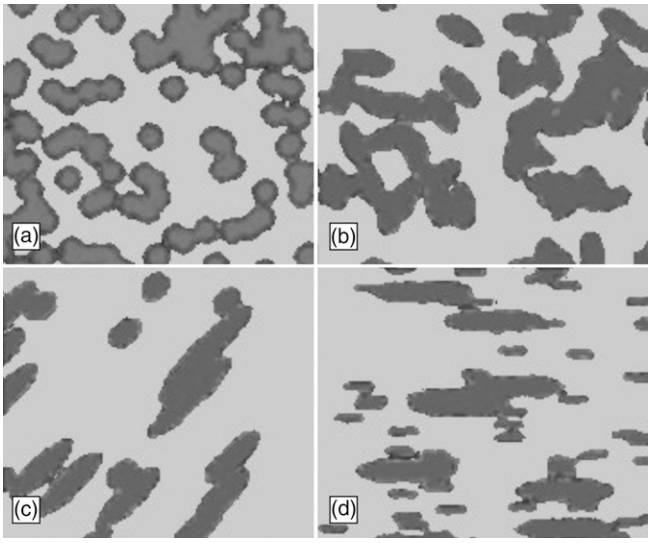

Fig. 3. Examples of grain shapes, alignments, and sizes generated using the ellipse algorithm: (a) rounded; (b) randomly oriented elongated; (c) aligned elongated; (d) aligned elongated with bimodal size distribution

and sizes can be generated (Fig. 3). In addition, the orientation of the elongated axis can be specified to generate foliation textures. The shapes were kept simple to reduce complexity and uncertainty in the model. All textures generated by the ellipse algorithm were simplifications of real rock textures in order to highlight the interactions between mineral grains in a clearly definable way.

Mineral-specific strength information was necessary to accomplish the parametric analysis previously described. Published estimates were available (Li et al. 2003; Chen et al. 2007), but a more rigorous investigation of published data was undertaken to substantiate the input values determined for the parametric analysis. Reliable published values were selected, and a mineral-specific constitutive model was developed using published descriptions of mineral fracture behavior and calibration with laboratory strength data (Villeneuve et al. 2009).

The bilinear-ubiquitous joint (*FLAC*) constitutive model used for UCS and Brazilian tensile modeling was used, because it resulted in the most realistic results during calibration. This model allows an isotropic constitutive relationship or, alternatively, an anisotropic elastic and plastic model (directional strength with isotropic flow postpeak). Quartz is assumed to be isotropic in its stiffness and strength. Feldspar has some anisotropy in reality. This minor directional dependence was simulated by imposing a greater range of stiffness and strength to phenomenologically account for mineral orientation with respect to stress. There are sufficient directionality data for mica (Lama and Vutukuri 1978) to be treated as a transversely anisotropic mineral with respect to the strength parameters. The ubiquitous joints were assigned mica parallel properties, while the matrix was assigned mica perpendicular properties. The input parameters are summarized in Table 1, and peak and residual strength envelopes are shown in Fig. 4.

Numerical Two-Dimensional Brazilian Tensile Strength and UCS Testing

Model Characteristics

FLAC models were initiated using an orthogonal nodal grid, which can be subsequently deformed to correspond to nonorthogonal shapes (i.e., circles). The simple strength test models were created using an orthogonal base grid with the locations of the element corners or nodes randomly perturbed to add geometric heterogeneity to the grid. Sensitivity analysis of the element size showed a 0.1% difference in strength and strain results for tests with an element size of 0.25−1 mm. An element size of 0.5 mm was selected to best satisfy the ability to model rocks with a small grain size, while taking into consideration computational time constraints. The model configurations for the Brazilian tensile strength and UCS samples are as follows.

Brazilian tensile strength (BTS) test model parameters [Fig. 5(b)] are as follows:

- 0.05-m-diameter circle with circular 100 × 100 element grid.
- One element = 0.5 mm.
- Strain-softening failure criterion for intact rock.

Table 1. Summary of Selected *FLAC* Input Strength Parameters for Rock Modeling

	Cohesion (MPa)			Friction coefficients		Elastic moduli (GPa)		
Mineral	Peak	Residual	σ_t (MPa)	Base	Gouge	Shear	Bulk	Cohesion loss strain $\varepsilon \times 10^{-3}$
Quartz	109	5	34.0	0.1230	0.65	19.0–31.0	28–44	3.5–5.7
Feldspar	80–125	4–6	36.0	0.120–0.590	0.80	28.0–33.0	55–65	2.4–4.4
Mica parallel	48	2	4.5	0.310	0.43	5.8	169	8.3
Mica perpendicular	95	5	39.0	0.780	0.43	5.8	169	16.3

Int. J. Geomech. 2012.12:632-647.

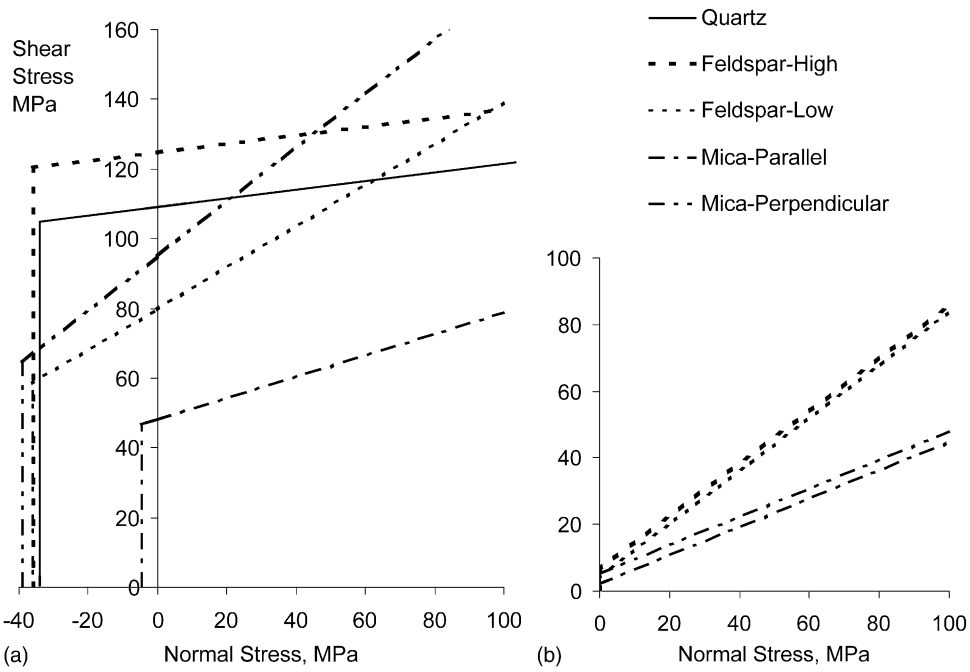

Fig. 4. (a) Peak Mohr-Coulomb strength envelope for quartz, feldspar, and mica; (b) residual Mohr-Coulomb strength envelope for quartz, feldspar, and mica

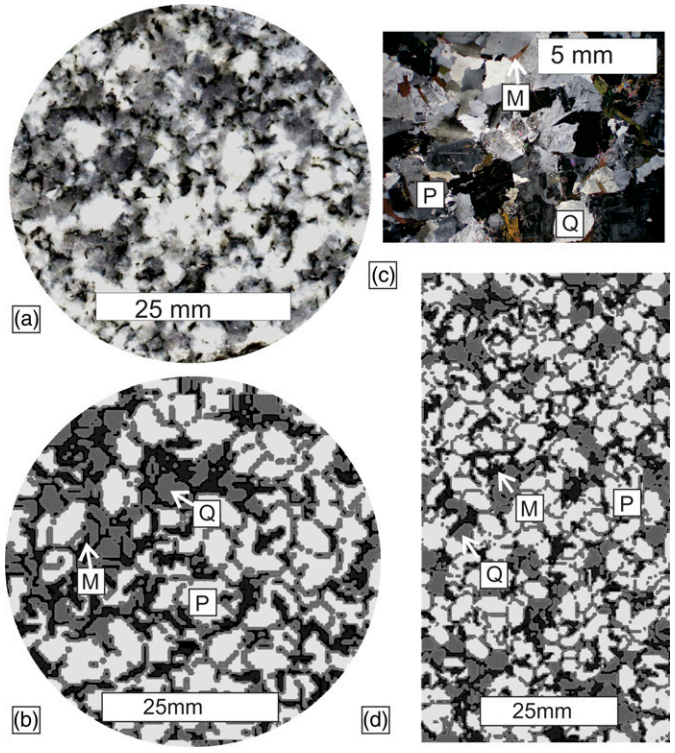

Fig. 5. (a) Brazilian sample of Stanstead granodiorite; (b) statistically modeled test in *FLAC*; (c) thin section of granodiorite; (d) modeled UCS test in *FLAC*; M = mica, P = plagioclase, Q = quartz

- Loading provided by applying an initial velocity distributed over an arc length $2\alpha = 0.32$ at the top and bottom ends of the circle instantaneously as well as incrementally applied. Velocity loading simulates servocontrolled Brazilian testing.
- Velocity decreased to a level where further decreases no longer affect the model results, at 1×10^{-9} m/step.
- FISH function is used to monitor unbalanced forces on the sample ends, which is turned into a stress, according to Eq. (4). The highest value the sample reaches is taken as the equivalent Brazilian tensile value for the test.
- FISH function also monitors maximum vertical and horizontal stresses in each element, failure mode, and step at which failure the occurred.

$$\sigma_\theta = -\frac{F}{\pi r_o t}\left[\frac{\sin 2\alpha}{\alpha} - 1\right] \tag{4}$$

where F = total applied load, t = sample thickness, r_o = distance from the center, and 2α = arc length over which the applied force is assumed to be radially distributed (Vutukuri et al. 1974).

The UCS numerical model parameters [Fig. 5(d)] are as follows:

- 0.05× 0.1 m size with 100 × 200 element grid.
- One element = 0.5 mm.
- Strain-softening failure criterion for intact rock.
- Loading provided by an applied initial velocity only at the top and bottom boundary. Velocity loading simulates servocontrolled UCS testing.
- Velocity decreased to the level where further decreases no longer affect model results, at 1×10^{-9} m/step.
- FISH function is used to monitor unbalanced forces on the sample ends, which is turned into a stress over the area. The highest value the sample reaches is taken as the equivalent UCS value for the test.
- FISH function also monitors maximum vertical and horizontal stresses in each element, failure mode, and step at which the failure occurred.

The rock analog simulation algorithm was used to simulate real rock textures, for example, the texture and the analog to the rock shown in Fig. 5. The constitutive model previously described was used to determine the mineral-specific input parameters used in the bilinear ubiquitous-joint constitutive model in *FLAC* (*FLAC*). Variability was introduced on a grain basis by randomly selecting

Int. J. Geomech. 2012.12:632-647.

Table 2. Properties of Samples Used for Parametric Analysis and Strength Testing Results

Sample	Mica (percentage)	Quartz (percentage)	Feldspar (percentage)	Grain size (mm)	Anisotropy type	Peak (MPa)	Systematic damage initiation point (MPa)	Brazilian tensile strength (MPa)
M1	5	20	75	4	None	168	114	18.9
M15	6	90	4	4	None	198	129	—
M2	16	16	68	4	None	141	107	16.0
M3	23	16	61	4	None	137	108	15.1
Q1	10	41	49	4	None	158	119	15.9
Q2	6	70	24	4	None	178	119	20.2
Q3	3	85	12	4	None	225	124	21.9
Q35	3	88	10	4	None	217	137	22.6
Q36	3	93	4	4	None	246	143	—
Q37	3	49	48	4	None	179	116	—
Q4	12	17	71	4	None	147	111	16.5
Q5	12	41	47	4	None	154	124	15.9
Q6	12	68	20	4	None	163	127	16.5
Q65	11	81	8	4	None	182	124	17.8
Q7	12	84	4	4	None	185	136	16.7
G15	9	23	68	3	None	155	124	—
G2	9	23	68	4	None	149	120	11.1
G25	8	24	68	6	None	153	121	—
G3	8	23	69	8	None	161	112	11.3
MPOg	11	24	65	3	>1 cm spaced	137	109	16.5
CC	29	35	36	4	<1 cm spaced	131	104	16.2

input parameters within a 5% range of the input parameters, except for feldspar, which has a 20% variation to account for anisotropy. Additional variability was introduced on an element basis by randomly selecting input parameters within a 5% range of the grain-specific input parameters. This variability simulates the grain scale variability because of differences in strength between grains of the same mineral, as well as intragranular variability because of crystal scale heterogeneity.

Numerical Strength Testing Results

Simulated uniaxial compression and Brazilian tests (approximated by plane strain two-dimensional [2D] simulations) were carried out. Model testing results were compared with mineralogy, grain size, and anisotropy to investigate the impacts of changing each characteristic on strength and systematic damage initiation as follows (Table 2, Fig. 6):

- Mineralogy;
- Variation in mica content (M1−M3);
- Variation in mica, quartz, and feldspar content (Q1−Q2);
- Variation in quartz to feldspar ratio at low mica content (∼3%, Q3−Q37); and
- Variation in quartz to feldspar ratio at high mica content (∼12%, Q4−Q7).
- Grain size; and
- Variation in size of all mineral grains (G2−G5).
- Anisotropy.
- Alignment of mica grains with variation in spacing of aligned micas (MPOg, CC).

The strength test output values used in the investigation are the peak strength, the systematic damage initiation point (CI), which is the stress at which new microfractures are generated (Diederichs and Martin 2010), and the BTS (Table 3). The ratios of CI to UCS (Eberhardt et al. 1998; Diederichs et al. 2004) and UCS to BTS were used as indicators of lower-bound strength.

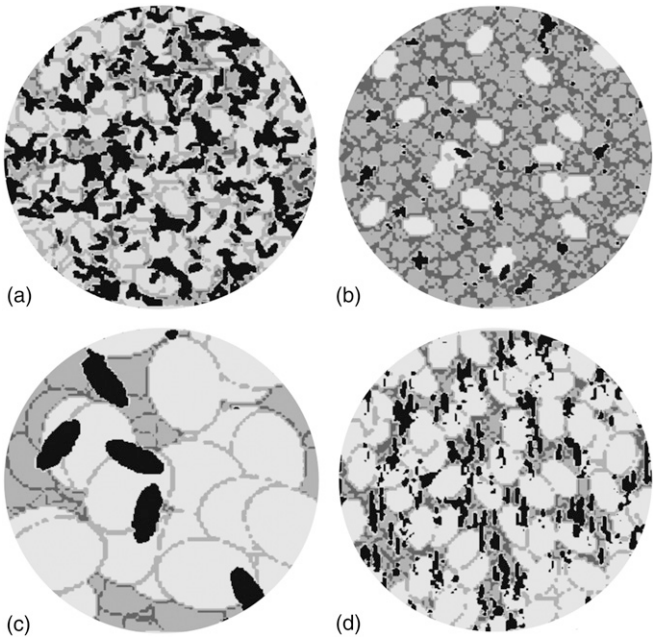

Fig. 6. Images of a selection of modeled samples from Table 2: (a) M3; (b) Q3; (c) G4; (d) MPOg; mineralogy is represented as in Fig. 5

Mica Content

Increasing mica content decreases peak compressive strength, although damage initiation is not impacted significantly by increasing mica content. BTS also declines with increasing mica content, and as such the ratio of UCS to BTS does not reflect this change (Fig. 7). The ratio of CI to UCS increases, although this is not because of an increase in initiation strength but rather a decrease in peak strength.

Int. J. Geomech. 2012.12:632-647.

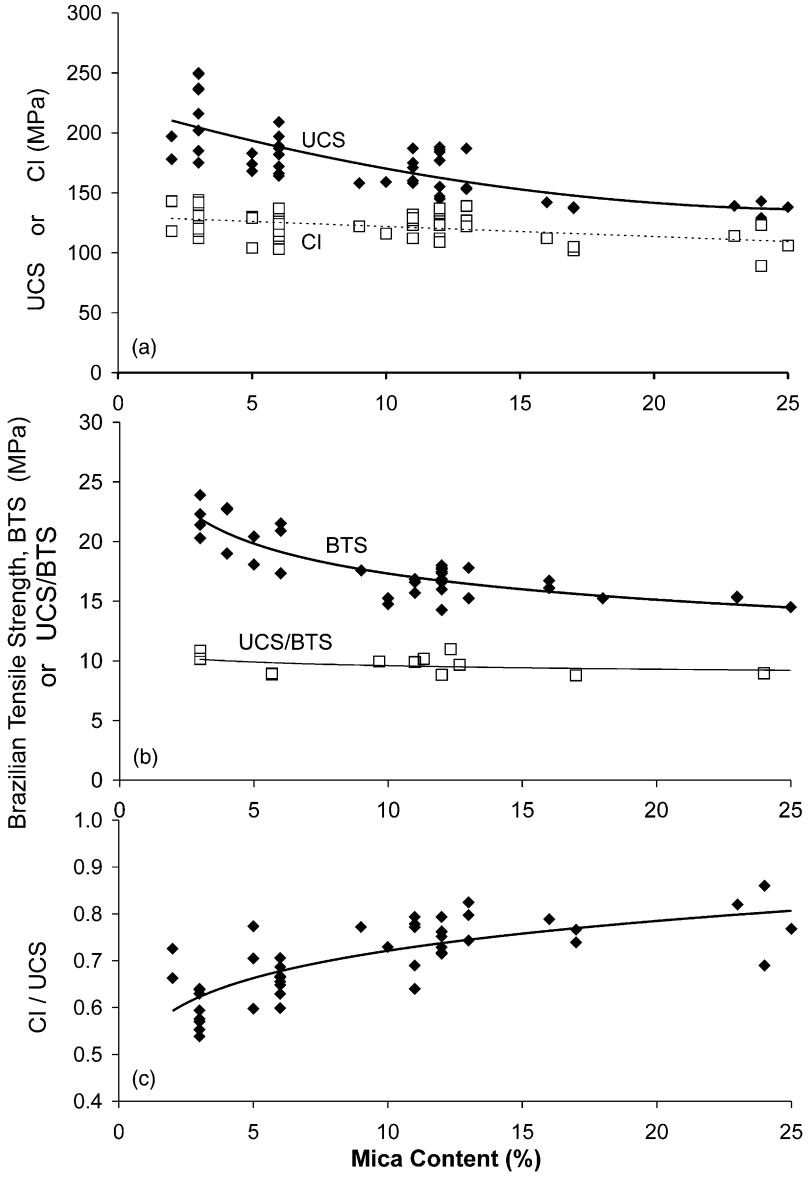

Fig. 7. (a) UCS and systematic damage initiation threshold versus mica content; (b) Brazilian tensile strength and ratio of UCS to Brazilian versus mica content; (c) ratio of CI to UCS versus mica content

Quartz to Feldspar Ratio

Increasing the quartz to feldspar ratio leads to a strength increase, regardless of mica content. This is accompanied by a slight increase in the UCS to BTS ratio and a decrease in the CI to UCS ratio (Fig. 8). The impact of the quartz to feldspar ratio on strength is more pronounced for low mica contents. At higher mica contents, the peak strength is controlled by the mica.

Grain Size

Compressive strength shows an initial drop with increasing grain size with a strength plateau above a critical dimension. Indirect tensile strength will increase with increased grain size. CI shows a minor decrease with increasing grain size, although the scatter makes trends in the ratio of CI to UCS less conclusive. The UCS to BTS ratio shows a dramatic decrease with grain size (Fig. 9).

Anisotropy

There is a slight decrease in UCS strength and varying indirect tensile strength with anisotropy. There is a general decrease in the UCS to BTS and CI to UCS ratios with anisotropy (Fig. 10). Anisotropic samples with thick lithons (cleavage spacing) show an increase in BTS.

Discussion

Fracture Behavior

Mineral-specific fracture behavior described in Li et al. (2003), Tapponnier and Brace (1976), Li (2001), and Wong (1982) was also observed in the 2D *FLAC* UCS models. Fig. 11 demonstrates some of the fracture processes typically observed in all samples given in Table 2. Micas were found to induce failure in the surrounding stiffer, albeit stronger, feldspars in the simulated samples [the mica grain inducing fracture through the adjacent feldspar grains in the upper-center of Fig. 11(a)] and in laboratory UCS testing of granite (Li 2001). Mica content was not found to impact CI, but higher concentrations may provide more potential for crack interaction and yield once initiation begins. Tensile fractures propagating through feldspars can be offset by more compliant mica grains in

Int. J. Geomech. 2012.12:632-647.

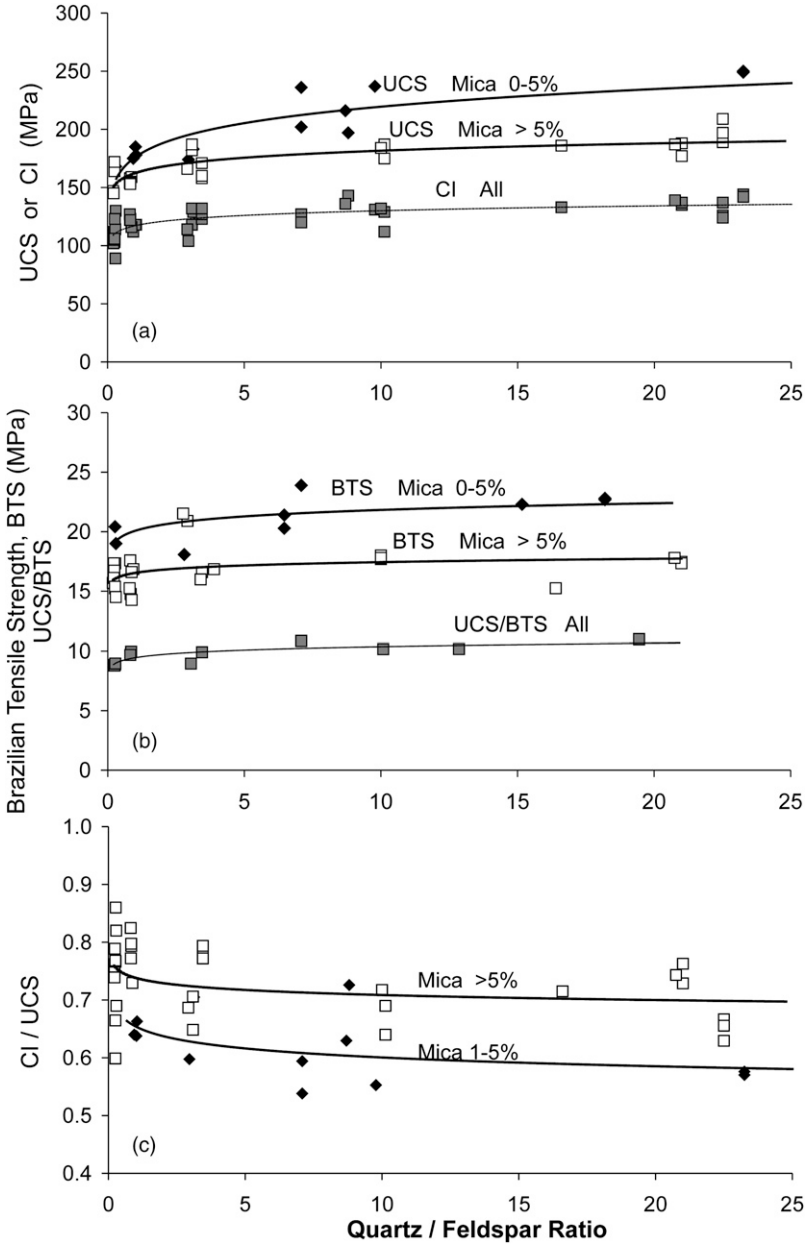

Fig. 8. (a) UCS and CI versus quartz to feldspar ratio categorized according to mica content; (b) Brazilian tensile strength and ratio of UCS to Brazilian versus quartz to feldspar ratio for mica content <10%; (c) ratio of CI to UCS versus quartz to feldspar ratio categorized according to mica content

the simulated samples and during laboratory UCS testing of granite (Tapponnier and Brace 1976; Li 2001). Anisotropy was found to control the location and orientation of the yield surface in simulated UCS tests [Figs. 11(d–f)]. Grain boundaries can act as both fracture initiators [the fractures around the feldspar grains in the lower center of Fig. 11(a)] and fracture inhibitors. Tensile fractures propagating through feldspars were halted at the softer and slightly weaker grain boundary [on the right of Fig. 11(a), slightly above the center, the fracture propagating up within a feldspar and halting at the grain boundary] in the simulated rocks as well as during laboratory UCS testing of granite (Li 2001; Martin 1994). Discrete discontinuum fracture processes, such as the loss of cohesion between adjacent grain boundaries, were not explicitly modeled using this continuum code; this, however, presents fracture mechanisms worth further exploration using codes capable of simulating these processes. The shear failure plane that develops in the sample at the peak [seen most clearly in the strain plots in Figs. 11(c and f)] was oriented similarly to the shear planes observed in the laboratory samples.

Modeled Laboratory Strength

The mineralogy parametric analysis results show that strength decreases with mica content and increases with the quartz to feldspar ratio. The impact of mica content on strength was less pronounced at higher mica contents, suggesting that beyond a particular mica content (~15%), increasing the mica content does not significantly impact peak strength, as seen in laboratory UCS testing (Prikryl 2001). Similarly, the impact of the quartz to feldspar ratio was less pronounced at a higher quartz to feldspar ratio. Similar positive

Int. J. Geomech. 2012.12:632-647.

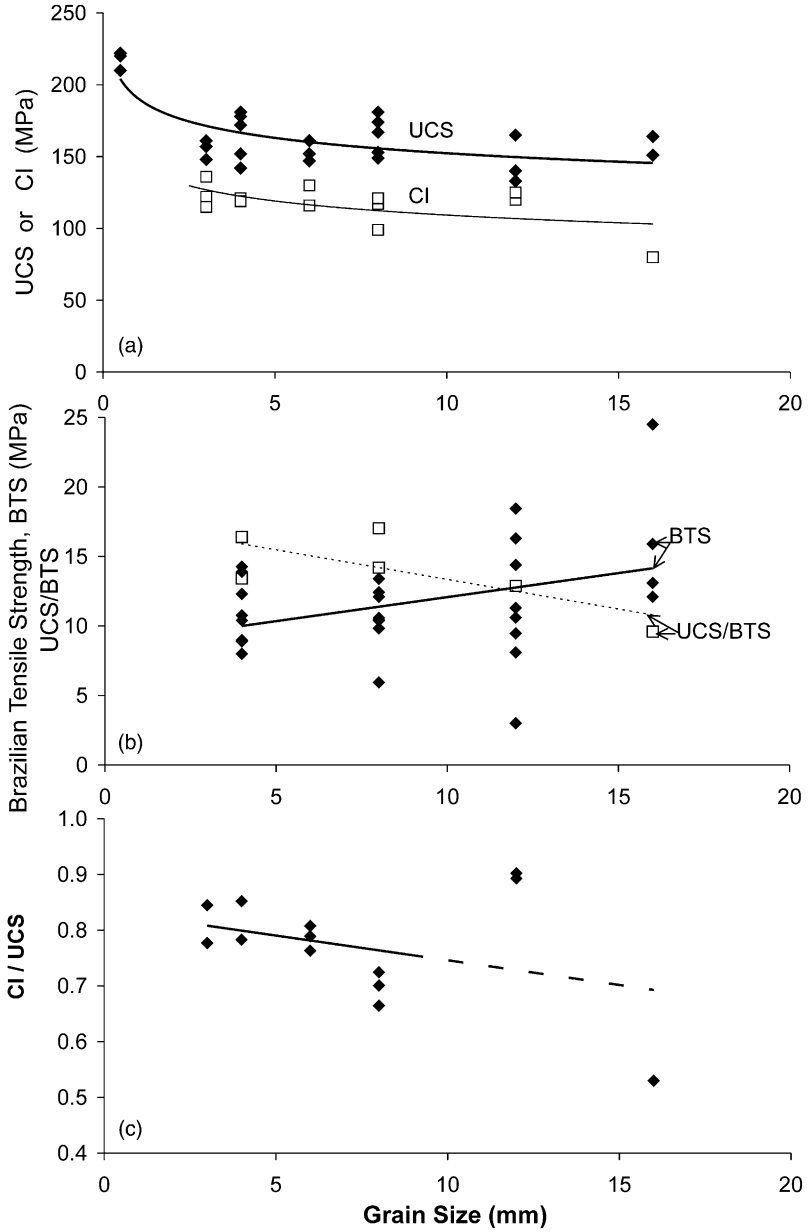

Fig. 9. (a) UCS and CI versus grain size; (b) Brazilian tensile strength and ratio of UCS to Brazilian versus grain size; (c) ratio of CI to UCS versus grain size

relationships were found in laboratory testing of granitic rocks (Tuğrul and Zarif 1999; Göransson et al. 2004).

The decreasing peak strength trend with increased grain size likely arises from the decreased proportion of grain boundaries, which act as damage inhibitors in modeled and laboratory samples (Li 2001; Martin 1994). The large pegmatitic grains will not initiate fractures easily, although fractures will be initiated at the grain boundaries and in mica grains, as shown in Fig. 11(a). Considerable stress is required for the initiated fractures to propagate across the boundaries and into the pegmatitic grains, where they propagate freely and induce failure of the sample. In smaller-grained samples, the ratio of grain boundary to grain interior is greater, providing more opportunity for fractures to initiate but reducing the ability of these fractures to propagate through the sample. If preexisting defects were included in the model, they would initiate fractures within the grains, which could easily propagate across the grains, without the need for fractures to be initiated at grain boundaries, thereby further lowering the peak strength of large-grained samples.

The effect is similar for BTS testing, where strength scatter and average strength both increase because of the increased impact of single minerals on the strength as grains increase in size. For samples with very large grain sizes with respect to sample size, the strength will be highly dependent on which mineral is located in the center of the sample, where failure typically initiates. In these samples, whichever mineral is in the center will dominate the fracturing initiation process, and the sample strength will approach the strength properties of the mineral. In the parametric analysis, the samples were composed mostly of feldspars, resulting in sample strengths often approaching the strength of feldspar. The converse could be true if the dominant mineral was the weakest mineral.

Int. J. Geomech. 2012.12:632-647.

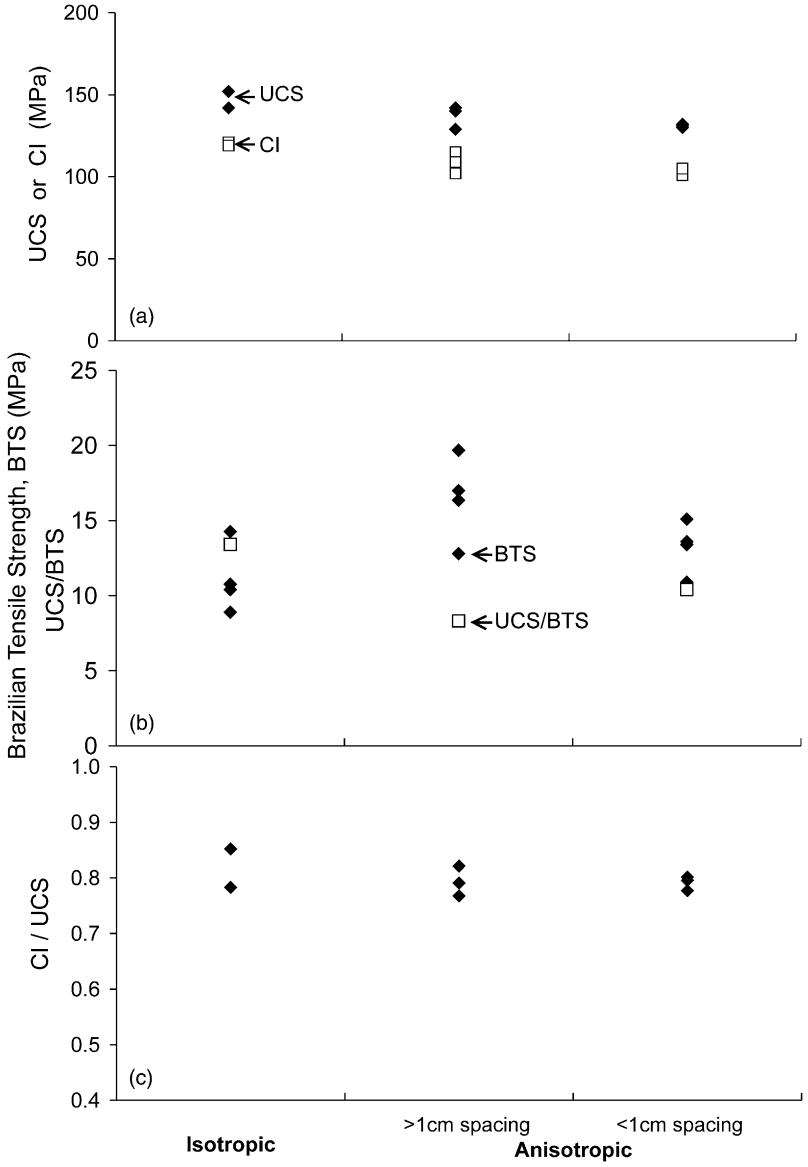

Fig. 10. (a) UCS and CI versus anisotropy aligned at 30° to the axis of loading; (b) Brazilian tensile strength versus anisotropy oriented parallel to the axis of loading and ratio of UCS to Brazilian versus anisotropy; (c) ratio of CI to UCS strength versus anisotropy aligned at 30° to the axis of loading

Grain anisotropy defined by aligned mica grains slightly decreases the peak strength, mostly because of the ability of the sample to benefit from the weakness planes defined by the aligned minerals. In the indirect tensile samples, the weakness plane must be exactly oriented in the center of the sample, where failure typically initiates, in order for the sample to benefit from it. In most samples this was not the case, and BTS strength actually increased because of the failure initiating and propagating almost entirely through feldspar and quartz. Because of the particular sensitivity of the BTS with respect to the location of failure initiation, it should be used with care with anisotropic material, and conclusions based on test results may not be representative of behavior in the field.

Implications for Lower-Bound In Situ Strength and Brittleness

Because of the 2D nature of the model, crack suppression arising from feedback confinement in laboratory samples (Diederichs et al. 2004) does not occur in the UCS models. The systematic damage initiation stress was, therefore, a much higher ratio of the peak strength in the modeled samples than was shown for laboratory tests (i.e., those given in Diederichs et al. 2004). Regardless, the systematic damage initiation stress to peak strength ratios from the modeled laboratory tests highlight relationships between modeled fracture behavior and modeled strength.

At low mica content, systematic damage was initiated in the sample but required considerable additional stress to induce failure because of the lack of crack initiators in the form of mica grains. The same is true, to a lesser extent, with increasing the quartz to feldspar ratio, with the feldspar grains acting as fracture initiators with respect to quartz grains because of their weakness planes defined by cleavage. The systematic damage initiation threshold was lowered slightly with increased mica content and decreased quartz to feldspar ratio by the presence of more fracture initiators. Fracture propagation was much improved, as demonstrated by the lower-peak

Int. J. Geomech. 2012.12:632-647.

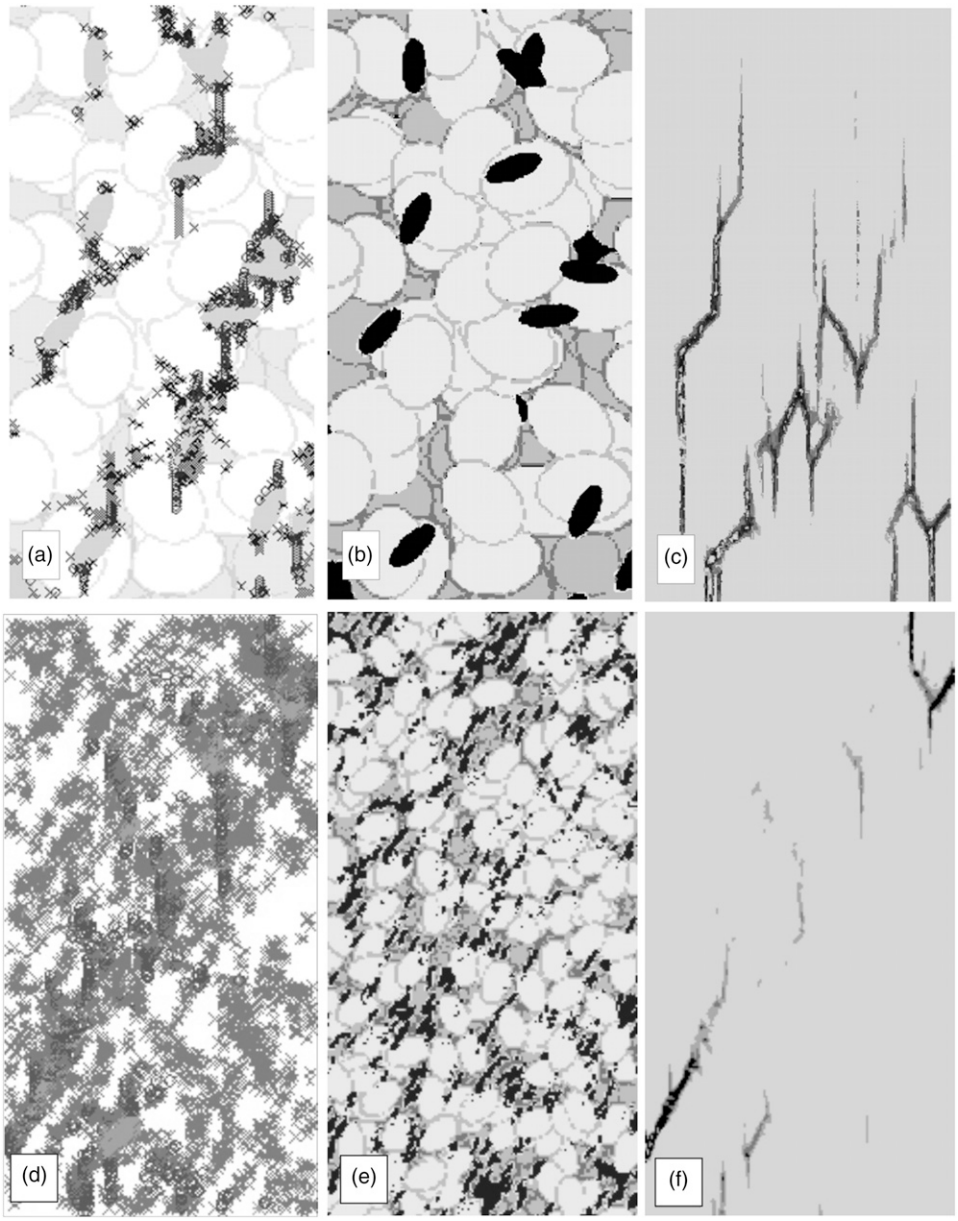

Fig. 11. *FLAC* output images of sample G4: (a) locations of failed elements; (b) mineralogy; (c) plastic strain; *FLAC* output images of anisotropic sample with <1 cm spacing: (d) locations of failed elements; (e) mineralogy; (f) plastic strain, where darker is a higher strain; mineralogy is represented as in Fig. 5

strength, by increased mica content and decreased quartz to feldspar ratio because of the greater potential for induced fractures to interact and the increase in grain scale heterogeneity because of a greater variety and distribution of minerals with different strengths and stiffnesses. This follows the relationship outlined by Diederichs et al. (2004) for mica content greater than 2%.

The ability of the numerical model to simulate fine grain rocks was limited by the size of the elements used. Grain sizes from 3 to 8 mm were demonstrated, which is considered coarse to pegmatitic. The lack of preexisting defects was likely also the reason for the inverse trend to that in Diederichs et al. (2004) for the same range in grain size. Eberhardt et al. (1999) state that a larger grain size does not impact the systematic damage initiation threshold but rather decreases peak strength. As previously stated, preexisting defects would decrease peak strength in the larger-grained samples, thereby increasing the CI to UCS ratio.

The relationship between the ratio of systematic damage initiation threshold to peak strength and anisotropy is not as well-defined at the relationship with peak strength.

Brittleness, as measured by the ratio of BTS to UCS is only slightly influenced by mineralogy, suggesting that it is not a suitable indicator of fracture behavior in the models. It shows a decreasing trend with grain size because of the lack of preexisting defects and the influence of single intact grains on indirect tensile strength, as previously discussed. The relationship to anisotropy is complex, arising from the high dependence of indirect tensile strength on the location of minerals making up the layers in the anisotropy and the induced tensile stress field within the sample. It is likely not a suitable indicator of failure behavior for samples with widely spaced anisotropy.

Int. J. Geomech. 2012.12:632-647.

Two-Dimensional Numerical Modeling of the Chipping Process during Tunnel-Boring Machine Excavation

Model Configuration

The excavation process for a hard rock TBM involves roller cutters applying cyclical pressure on concentric rings in the tunnel face with fragmentation occurring between cutter tracks or kerfs (Fig. 12). The chipping process is the basis for understanding rock cutting during TBM excavation and is postulated to be accomplished by inducing tensile fractures into the rock, which then propagate parallel to the tunnel face. The fractures induced into the rock act to precondition the rock, making it easier to excavate during subsequent rotations of the cutterhead, while the fractures propagating parallel to the tunnel face will coalesce with similar fractures induced by adjacent cutters to create chips. Grinding occurs when fractures do not propagate through the rock and only fines are generated. Efficient TBM penetration, as a function of thrust applied to the cutters and the resulting penetration rate, relies on ensuring that a chipping mechanism dominates over a crushing or plastic deformation mechanism under the cutter (Fig. 13).

Numerical modeling of rock cutting was undertaken using the rock simulation algorithm. The two-cutter numerical model shown in Fig. 14(a) has 0.5 mm elements in the rock block, requiring a grid 180 elements wide × 240 elements tall. The 0.5 mm elements are the same size as the elements used in the laboratory strength testing simulations. Each cutter is represented by half a cutter to make computation more efficient. Roller boundary conditions were applied to the vertical sides of the cutters to ensure that they were only displaced vertically. Roller boundaries were also applied to the sides and bottom of the rock block to allow vertical and horizontal deformation, but there was no displacement of the block. The contact between the cutter and the rock is a joint interface that has no shear or tensile strength, but does exhibit frictional properties to simulate the independent steel cutter and rock block. The joint stiffness moduli were calculated as $5e^{13}$ Pa using Eq. (5), based on the stiffness and dimensions of elements on either side of the joint

$$\max \frac{\left[K + \frac{4}{3}G\right]}{z} \tag{5}$$

where K and G = bulk and shear modulus, respectively, z = element width, and max refers to using the maximum value if surrounding elements have different stiffness moduli or element sizes.

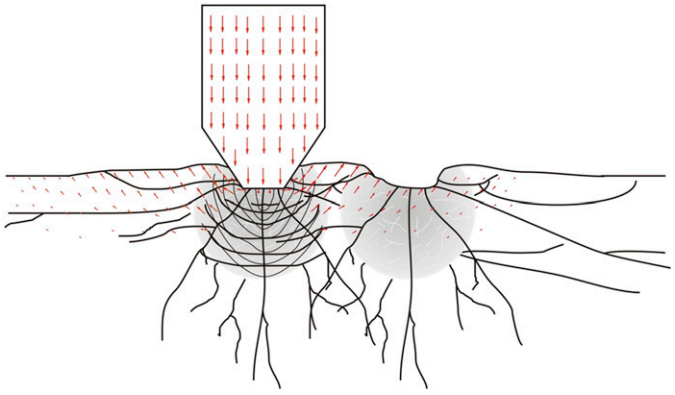

Fig. 12. Schematic cross section of tunnel-boring machine cutter and tunnel face rock showing force vectors: crushed zone (shaded), induced fractures, kerf (trough next to cutter), and generated chips

Four cutter passes were simulated by incrementally (1 mm) moving the cutter into the rock [Fig. 14(a)] and then applying a sinusoidal velocity gradient over one cycle, with maximum and minimum velocity of $5e^{-7}$ and $-5e^{-7}$ m/step, respectively, for 50,000 steps, which resulted in stress at the cutter tip (Fig. 15) that is comparable with the stress at real three-dimensional TBM cutter tips (Table 3). Rolling forces (out-of-plane) on the kerf edge could not be simulated in this 2D model. The texture-generating algorithm previously described was used to simulate rock [Fig. 16(a and b)], while steel properties were used for the cutters. After four cutter passes (for a total of 4-mm penetration), the accumulated plastic strain [Fig. 16(c)], representing fractures, was used to determine the chip preconditioning area (length × depth) below each cutter. The chip preconditioning area was used as the main indicator of chipping performance in the analysis of the numerical model results.

Table 3. Summary of Contact Area, Force, and Stress at Tip of Three- and Two-Dimensional Cutters with a 1-mm-Deep Kerf

Dimensions	Contact area (m^2)	Force at tip (N)	Stress at tip (MPa)
Three	8.3×10^{-4}	2.63×10^{5}	316
Two	3×10^{-2}	9.40×10^{6}	316

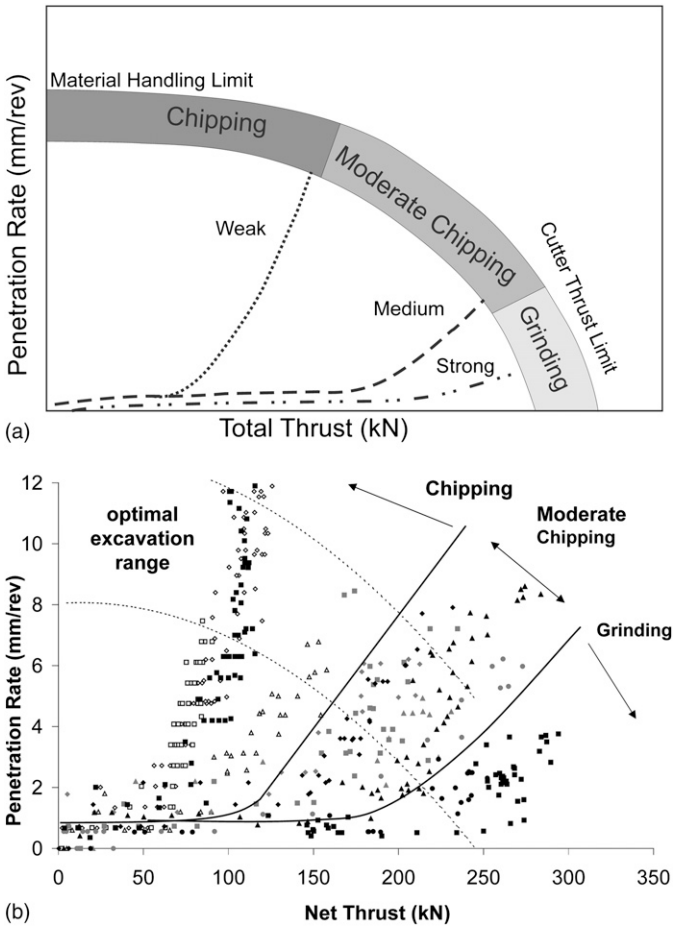

Fig. 13. Penetration versus thrust graphs: (a) schematic showing relative rock strengths and regions of chipping performance; (b) start-up test data showing chipping performance in different rock types; symbols represent individual tests

Int. J. Geomech. 2012.12:632-647.

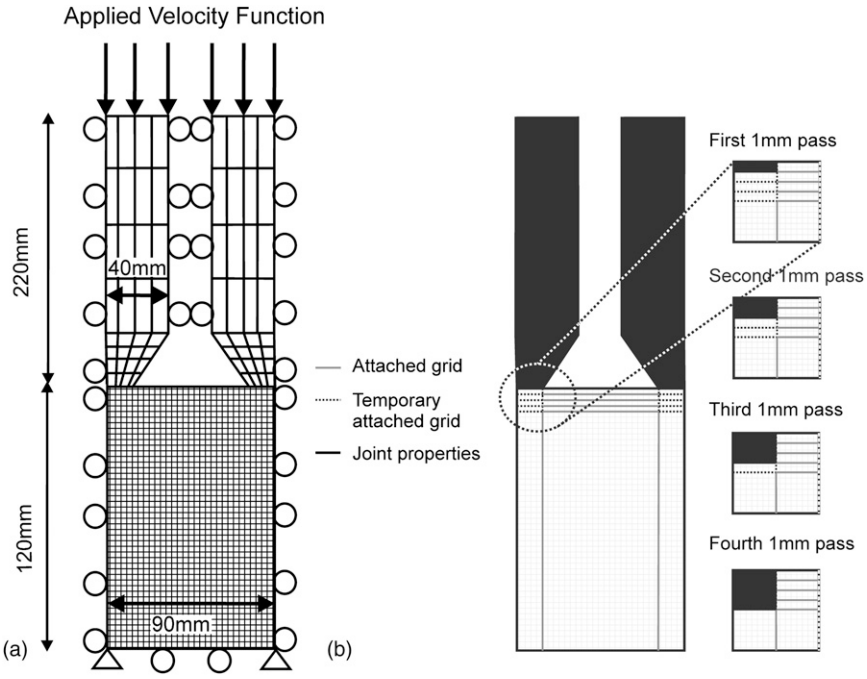

Fig. 14. (a) Schematics of two-cutter model showing dimensions and boundary conditions (grid not to scale); (b) cutter advance in 1-mm increments to simulate 1-mm-deep kerf: the rock grid was cut during grid generation to allow the subsequent progression of the cutters: the joints subsequently used along the cutter boundary (with joint properties) were temporarily attached, then given joint properties at the appropriate time: other joints not used along the cutter boundary (but necessary in grid generation) were attached throughout the simulation

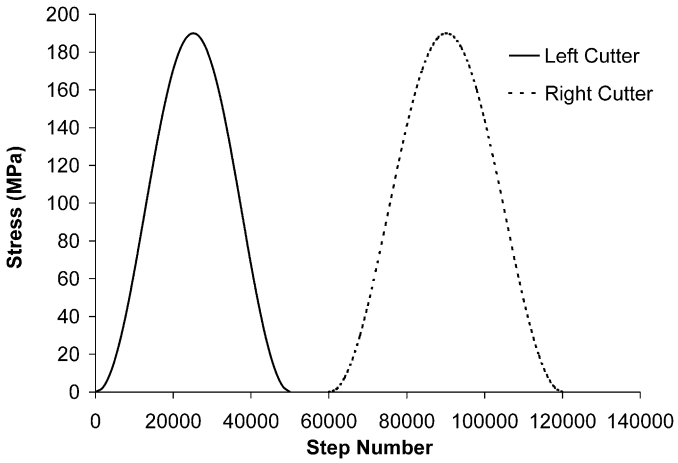

Fig. 15. Output of elemental stress at the cutter/rock interface resulting from the applied velocity functions in the elastic model

Numerical Chipping Process Results

The geomechanical characteristics given in Table 2 were used in the two-cutter model to investigate the impact of different geomechanical characteristics on the chipping performance. The fracture behavior, magnitude of chip creation, and depth and length of preconditioning observed in the numerical models were used to make conclusions regarding the impact of different characteristics on the chipping performance. The results show clear relationships between geomechanical properties and the chip preconditioning area, and therefore chipping performance.

The mineralogy was investigated in terms of mica content and quartz to feldspar ratio. These data show that the chipping performance increases with mica content and with increased quartz to feldspar ratio (Fig. 17). Chipping performance increases with increasing grain size and with widely spaced anisotropy but decreases with closely spaced anisotropy (Fig. 18).

Discussion

The multiphase strength envelope developed for low-confinement conditions at excavation boundaries (Fig. 19) demonstrates that rock strength at excavation boundaries is dominated by systematic damage initiation mechanisms and by fracture propagation mechanisms (Diederichs 2003). In the case of TBM excavation, the chipping process occurs at low confinement, except in the limited area directly below the cutter, and employs a mechanism similar to spalling. Extensile fractures initiated by the cutters are sensitive to the systematic damage initiation threshold, and the ability of the fractures to propagate parallel to the tunnel face is sensitive to material and physical aspects, such as scale effects, preexisting damage as a result of unloading or stress rotation, heterogeneity, and induced local tension (Diederichs et al. 2004; Diederichs 2003).

For the chipping mechanism, a high systematic damage initiation threshold [Fig. 20(a)] will make fracture initiation into the rock difficult, ultimately leading to grinding dominating over chipping [Fig. 20(b)]. For rocks with low systematic damage initiation threshold [Fig. 20(c)], chipping will dominate and the ability to propagate fractures will determine how efficient that chipping will be [Fig. 20(d)].

The ability for fractures to propagate once they have been induced is evident from the CI to UCS ratios and is shown to play a dominant role in TBM excavation. The combination of low systematic damage initiation threshold and increased ability to propagate fractures will increase chipping performance, as is the case with increasing mica content in Figs. 7 and 17 and conversely for

Int. J. Geomech. 2012.12:632-647.

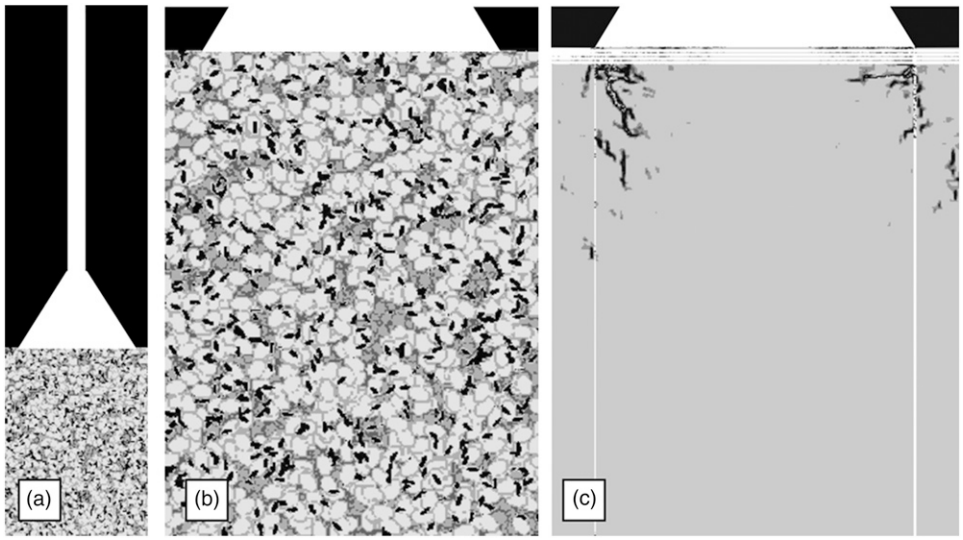

Fig. 16. *FLAC* model outputs of (a) sample G2; (b) showing rock texture; (c) showing strain after four cutter passes, representing preconditioning in the rock arising from generated fractures; mineralogy is represented as in Fig. 5

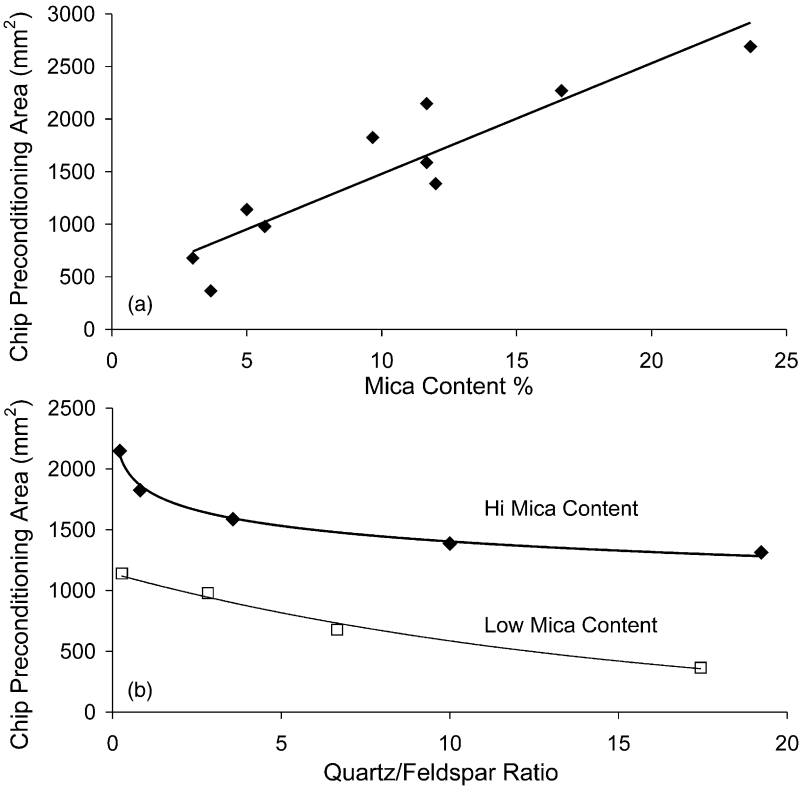

Fig. 17. Chip preconditioning area versus (a) mica content; (b) quartz to feldspar ratio categorized according to mica content

increasing the quartz to feldspar ratio in Figs. 8 and 17. Low mica content and high quartz to feldspar ratio will both lead to high systematic damage initiation thresholds and poor fracture propagation, resulting in grinding dominated excavation (Fig. 17), as in Scenarios A and B of Fig. 20(b). High mica content and low quartz to feldspar ratio will both lead to slightly lower systematic damage initiation thresholds and much improved fracture propagation, resulting in chipping dominated excavation (Figs. 17), as in Scenarios C and D of Fig. 20(d).

The ability to propagate fractures in large-grained samples is much more pronounced in the two-cutter model than in the UCS model. This is demonstrated by the relationship between lower systematic damage initiation threshold and increased chipping performance (Figs. 9 and 18). The increased ability to propagate fractures in rocks with larger grain sizes is similar to moving from Scenario C to D in Figs. 20(c and d). It may be that during TBM cutter excavation, fracture propagation parallel to the tunnel face is strong enough to propagate fractures across grain boundaries,

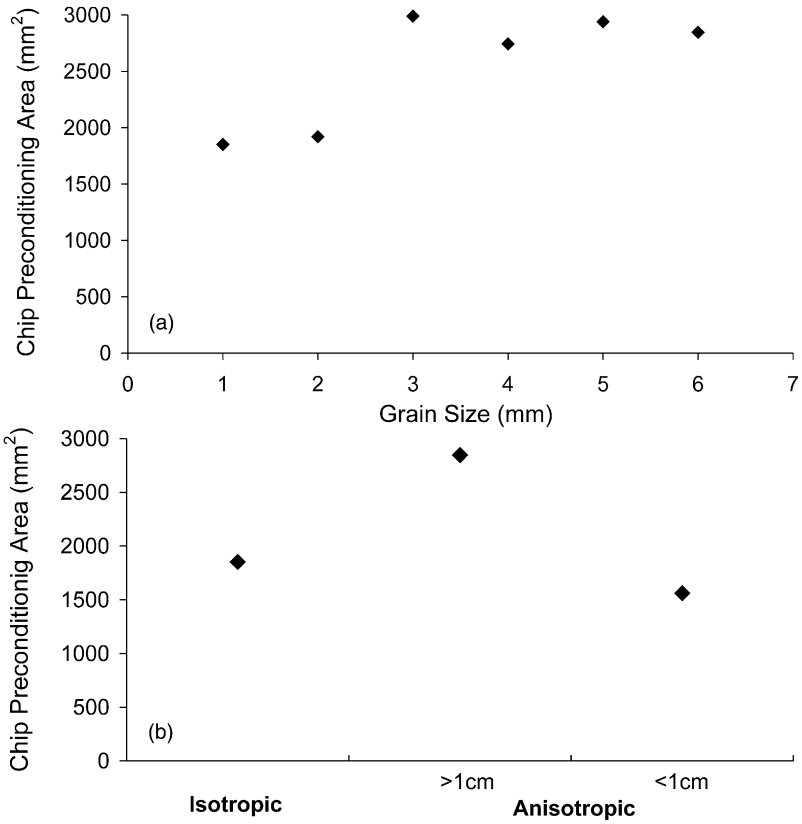

Fig. 18. Chip preconditioning area versus (a) grain size; (b) anisotropy

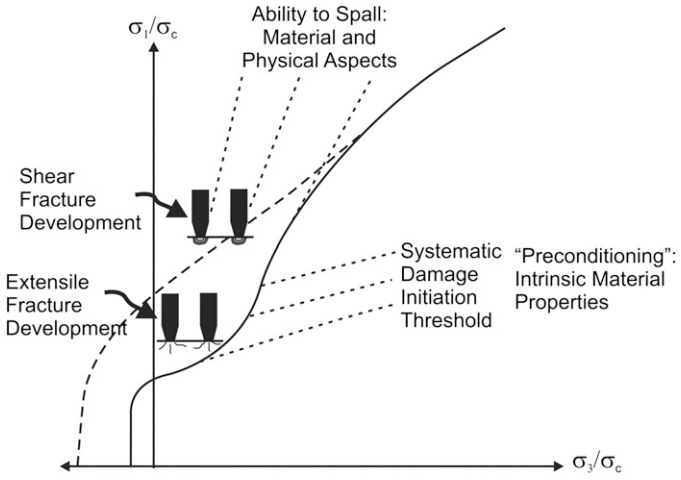

Fig. 19. Schematic composite in situ strength envelope for hard rock showing zones of tunnel-boring machine cutter chipping performance (graphed according to Diederichs 2003 and Diederichs et al. 2004)

without necessitating preexisting internal grain damage. This should be investigated by adding preexisting damage to the simulated mineral grains.

The ratio of systematic damage initiation and peak strength is not as clearly linked to chipping performance for rocks with anisotropy, because the anisotropy is a spatially oriented plane of weakness, which impacts strength testing and the chipping mechanism differently. The widely spaced anisotropy has been shown to improve chipping performance when compared with an isotropic rock with similar mineralogy (Fig. 18). The widely spaced weakness planes allow fractures to propagate into the rock and increase the preconditioning area, similar to moving from Scenario C to D in Figs. 20(c and d). The closely spaced anisotropy has been shown to reduce chipping performance (Fig. 18) by distributing the induced fractures along several closely spaced weakness planes, dissipating the energy that drives the fractures to propagate and generate chips, similar to moving from Scenario D to C in Figs. 20(c and d).

Conclusions

A methodology developed to simulate realistic rock analogs was used in a parametric analysis of the impact of geological characteristics on modeled strength tests. A texture generation algorithm was created to build ellipses representing three major rock-forming minerals. Mineral-specific constitutive models were developed and calibrated using published data and comparison with laboratory testing values and behaviors. The finite-difference numerical modeling software *FLAC* was programmed to apply the texture generation algorithm and the mineral-specific constitutive model to generate rock analogs for BTS and UCS tests in two dimensions. The methodology presented herein could be used for different sized simulated laboratory tests to investigate scale effects.

The results of parametric analysis of different mineralogies, grain sizes, and anisotropy show that fracture behavior in the model simulates fracture behavior observed in rock during laboratory testing. The strength values show trends that have been supported in published laboratory strength tests. This approach can be used to investigate fracture behavior at the grain scale and its dependence on grain scale heterogeneity.

Int. J. Geomech. 2012.12:632-647.

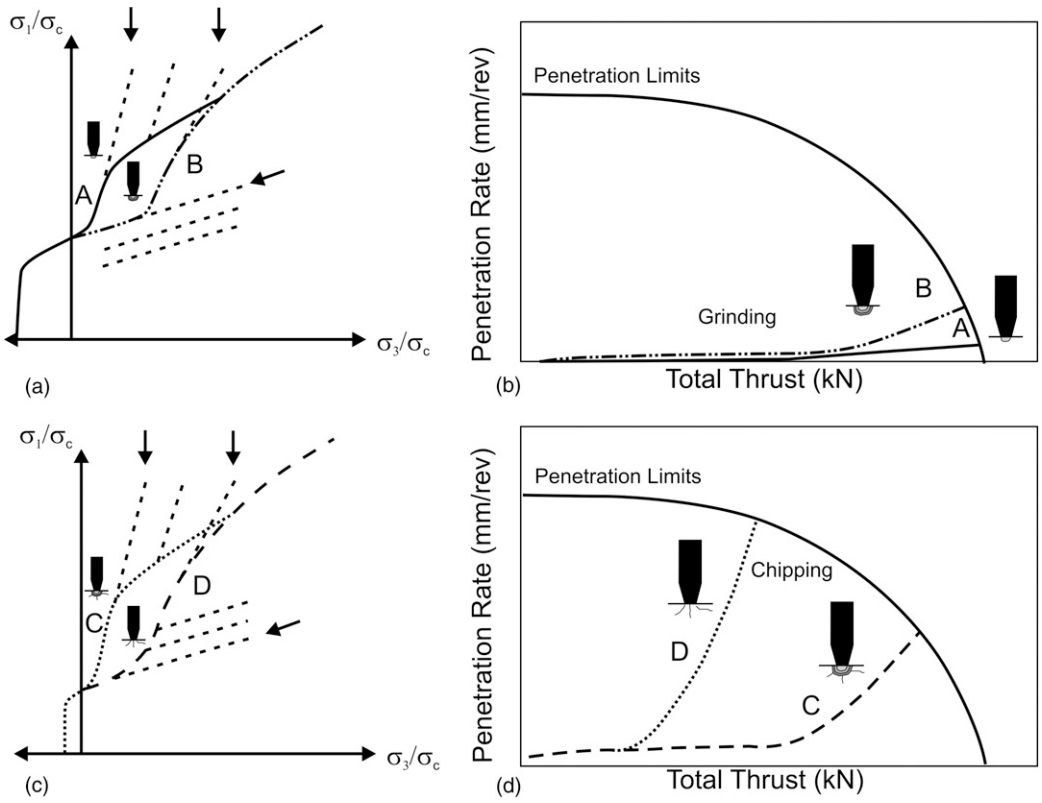

Fig. 20. Relationship between combinations of damage initiation thresholds and ability to spall with chipping performance: (a) and (b) high systematic damage initiation threshold leads to grinding; (c) and (d) low systematic damage initiation threshold leads chipping

The modeling of the TBM excavation process using the rock simulation algorithm has demonstrated the impact on the chipping process of mineralogy, grain size, and anisotropy. It has shown, most importantly, that increased mica content and decreased quartz to feldspar ratio will lead to a chipping rather than grinding dominated chipping process. This approach can be used to infer the impact of different rock types on the chipping process as well as to gain a better understanding of fracture initiation, fracture propagation, and chip creation below the cutter tip.

Taking care to create run-time efficient model geometries, this approach could be used to model other geometric configurations for laboratory strength tests or other rock mechanics processes. A three-dimensional version of this approach, using three-dimensional ellipsoids, could be used in numerous applications, such as modeling of excavations and three-dimensional processes. This approach could be improved by adding preexisting damage inside the grains as a fourth parameter for investigation.

Acknowledgments

Financial support was provided by Herrenknecht AG and a Postgraduate Scholarship from the Natural Science and Engineering Research Council (NSERC) of Canada.

References

Barton, N. (2000). *TBM tunnelling in jointed and faulted rock*, Balkema, Rotterdam, Netherlands.

Barton, N., Lien, R., and Lunde, J. (1974). "Engineering classification of rock masses for the design of tunnel support." *Rock Mech.*, 6(4), 189–239.

Bieniawski, Z. T. (1989). *Engineering rock mass classifications*, Wiley, New York.

Brace, W. F. (1960). "An extension of the Griffith theory of fracture to rocks." *J. Geophys. Res.*, 65(10), 3477–3480.

Brace, W. F. (1961). "Dependence of fracture strength of rocks on grain size." *Proc., 4th Sym. Rock Mech.*, H. L. Hartman, ed., American Association of Rock Mechanics, Pennsylvania State Univ., 99–103.

Bruland, A. (1998). "Hard rock tunnel boring." Ph.D. thesis, Univ. of Trondheim, Trondheim, Norway.

Castelli, M., Seatta, V., and Scavia, C. (2003). "Numerical study of scale effects on the stiffness modulus of rock masses." *Int. J. Geomech.*, 3(2), 160–169.

Chen, S., Yue, Z. Q., and Tham, L. G. (2007). "Digital image based approach for three-dimensional mechanical analysis of heterogeneous rocks." *Rock Mech. Rock Eng.*, 40(2), 145–168.

Coggan, J. S., Pine, R. J., Stead, D., and Rance, J. (2003). "Numerical modelling of brittle rock failure using a combined finite-discrete element approach: Implications for rock engineering design." *Proc. International Society of Rock Mechanics 2003—Technol. Roadmap Rock Mech.*, South African Institute of Mining and Metallurgy, Sandton, South Africa.

Diederichs, M. S. (2003). "Rock fracture and collapse under low confinement conditions." *Rock Mech. Rock Eng.*, 36(5), 339–381.

Diederichs, M. S., Kaiser, P. K., and Eberhardt, E. (2004). "Damage initiation and propagation in hard rock during tunnelling and the influence of near-face stress rotation." *Int. J. Rock Mech. Min. Sci.*, 41(5), 785–812.

Diederichs, M. S., and Martin, C. D. (2010). "Measurement of spalling parameters from laboratory testing." *Proc., Eurock 2010,* International Society of Rock Mechanics, Lausanne, Switzerland.

Eberhardt, E., Stead, D., Stimpson, B., and Read, R. S. (1998). "Identifying crack initiation and propagation thresholds in brittle rock." *Can. Geotech. J.*, 35(2), 222–233.

Int. J. Geomech. 2012.12:632-647.

Eberhardt, E., Stimpson, B., and Stead, D. (1999). "Effects of grain size on the initial and propagation thresholds of stress-induced brittle fractures." *Rock Mech. Rock Eng.*, 32(2), 81−99.

FLAC: Fast Langrangian Analysis of Continua 5 [Computer software]. Minneapolis, Itasca.

Göransson, M., Persson, L., and Wahlgren, C. (2004). "The variation of bedrock quality with increasing ductile deformation." *Bull. Eng. Geol. Environ.*, 63(4), 337−344.

Hoek, E. (1994). "Strength of rock and rock masses." *ISRM News J.*, 2(2), 4−16.

Illston, J. M., Dinwoodie, J. M., and Smith, A. A. (1979). *Concrete, timber and metals: The nature and behaviour of structural materials*, Van Nostrand Reinhold, Wokingham, U.K.

Kaiser, P. K. (2005). "Tunnel stability in highly stressed, brittle ground—Rock mechanics considerations for Alpine tunnelling." *Geologie und Geotechnik der Basistunnels am Gotthard und am Lötschberg*, vdf Hochschulverlag AG and der ETH Zürich, S. Löw, ed., 183−201.

Kaiser, P. K., McCreath, D., and Tannant, D. (1995). *Canadian Rockburst support handbook*, Geomechanics Research Centre and Canadian Mining Industry Research Organisation (CAMIRO), Sudbury, Canada.

Lama, R. D., and Vutukuri, V. S. (1978). *Handbook on mechanical properties of rocks*, Trans Tech Publications, Clausthal, Germany.

Li, L. (2001). "Microscopic study and numerical simulation of the failure process of granite." Ph.D. thesis, Univ. of Lulea, Lulea, Sweden.

Li, L., Lee, P. K. K., Tsui, Y., Tham, L. G., and Tang, C. A. (2003). "Failure process in granite." *Int. J. Geomech.*, 3(1), 84−98.

Liu, H. Y., Kou, S. Q., and Lindqvist, P. (2002a). "Numerical simulation of the fracture process in cutting heterogeneous brittle material." *Int. J. Numer. Anal. Methods Geomech.*, 26(13), 1253−1278.

Liu, H. Y., Kou, S. Q., Lindqvist, P., and Tang, C. A. (2002b). "Numerical modelling of rock fragmentation process induced by multiple indenters." *NARMS-TAC 2002: Mining and tunnelling innovation and opportunity: Proc., 5th North American Rock Mechanics Symposium and the 17th Tunnelling Association of Canada Conference : NARMS-TAC 2002,* R. Hammah et al., eds., Canadian Rock Mechanics Association (CARMA) and Tunnelling Association of Canada (TAC), Toronto, Canada.

Mahabadi, O. K., Cottrell, B. E., and Grasselli, G. (2010). "An example of realistic modelling of rock dynamic Problems: FEM/DEM simulation of dynamic Brazilian test on barre granite." *Int. J. Rock Mech. Min. Sci.*, 43(6), 707−716.

Martin, C. D. (1994). "The strength of massive Lac du Bonnet granite around underground openings." Ph.D. thesis, Univ. of Manitoba, Manitoba, Canada.

Martin, C. D., Kaiser, P. K., and McCreath, D. R. (1999). "Hoek-Brown parameters for predicting the depth of brittle failure around tunnels." *Can. Geotech. J.*, 36(1), 136−151.

Prikryl, R. (2001). "Some microstructural aspects of strength variation in rocks." *Int. J. Rock Mech. Min. Sci.*, 38(5), 671−682.

Rostami, J., and Ozdemir, L. (1993). "A new model for performance prediction of hard rock TBMs." *Proc., Rapid Excavation and Tunneling Conference,* Boston, 793−809.

Shen, B., et al. (2011). "FRACOD modeling of rock fracturing and permeability change in excavation-damaged zones." *Int. J. Geomech.*, 11(4), 302−313.

Sulem, J., and Cerrolaza, M. (2002). "Finite element analysis of the indentation test on rocks with microstructure." *Comput. Geotech.*, 29(2), 95−117.

Tang, C. A., and Kaiser, P. K. (1998). "Numerical simulation of cumulative damage and seismic energy release during brittle rock failure−Part I: Fundamentals." *Int. J. Rock Mech. Min. Sci.*, 35(2), 113−121.

Tapponnier, P., and Brace, W. F. (1976). "Development of stress-induced microcracks in westerly granite." *Int. J. Rock Mech. Min. Sci.*, 13(4), 103−112.

Tuğrul, A., and Zarif, I. H. (1999). "Correlation of mineralogical and textural characteristics with engineering properties of selected granitic rocks from Turkey." *Eng. Geol.*, 51(4), 303−317.

Villeneuve, M. C., Diederichs, M. S., Kaiser, P. K., and Frenzel, C. (2009). "Constitutive model for numerical modelling of highly stressed heterogeneous massive rocks at excavation boundaries." *Proc., 3rd Canada-USA Rock Mech. Sym.,* M. Diederichs and G. Grasselli, eds., Canadian Rock Mechanics Association (CARMA), Toronto.

Vutukuri, V. S., Lama, R. D., and Saluja, S. S. (1974). *Handbook on mechanical properties of rocks*, Trans Tech Publications, Clausthal, Germany.

Wong, T.-F. (1982). "Micromechanics of faulting in westerly granite." *Int. J. Rock Mech. Min. Sci. Geomech. Abstr.*, 9(2), 49−64.

Zhu, W. C., and Tang, C. A. (2004). "Micromechanical model for simulating the fracture process of rock." *Rock Mech. Rock Eng.*, 37(1), 25−56.